RSC Advances

PAPER

View Article Online
View Journal | View Issue

Cite this: *RSC Adv.*, 2022, **12**, 2485

Detection of free chlorine in water using graphene-like carbon based chemiresistive sensors†

Ana Zubiarrain-Laserna,[a] Shayan Angizi,[a] Md Ali Akbar,[a] Ranjith Divigalpitiya,[b] Ponnambalam Ravi Selvaganapathy[c] and Peter Kruse*[a]

Free chlorine is the most commonly used water disinfectant. Measuring its concentration during and after water treatment is crucial to ensure its effectiveness. However, many of the existing methods do not allow for continuous on-line monitoring. Here we demonstrate a solid state chemiresistive sensor using graphene-like carbon (GLC) that overcomes that issue. GLC films that were either bare or non-covalently functionalized with the redox-active phenyl-capped aniline tetramer (PCAT) were successfully employed to quantify aqueous free chlorine, although functionalized devices showed better performance. The response of the sensors to increasing concentrations of free chlorine followed a Langmuir adsorption isotherm in the two tested ranges: 0.01–0.2 ppm and 0.2–1.4 ppm. The limit of detection was estimated to be 1 ppb, permitting the detection of breaches in chlorine filters. The devices respond to decreasing levels of free chlorine without the need for a reset, allowing for the continuous monitoring of fluctuations in the concentration. The maximum sensor response and saturation concentration were found to depend on the thickness of the GLC film. Hence, the sensitivity and dynamic range of the sensors can be tailored to different applications by adjusting the thickness of the films. Tap water samples from a residential area were tested using these sensors, which showed good agreement with standard colorimetric measurement methods. The devices did not suffer from interferences in the presence of ions commonly found in drinking water. Overall, these sensors are a cost-effective option for the continuous automated monitoring of free chlorine in drinking water.

Received 11th November 2021
Accepted 12th January 2022

DOI: 10.1039/d1ra08264g

rsc.li/rsc-advances

Introduction

Free chlorine content is an important water quality parameter, because of its widespread use as a disinfectant for drinking water. It is added at the water treatment facility to remove pathogens (primary disinfectant) and to ensure that pathogens (*e.g.* bacteria and viruses) cannot re-contaminate the water during distribution (secondary disinfectant). This is because an isolated exposure to pathogens can lead to infection and have fatal consequences.[1–3] Continuous online monitoring of their presence and concentration in water is not straightforward, even though some limited progress has been made using solid state sensors.[4–6] Monitoring the concentration of added disinfectants is a viable alternative since their presence at a sufficiently high level implies the absence of pathogens.[7] In the pH range of drinking water the addition of commercial chlorine disinfectants (*e.g.* chlorine gas or bleach) results in an equilibrium between hypochlorous acid (HOCl) and hypochlorite (OCl^-).[8] Together they are known as free chlorine.[9] It is the most commonly used disinfectant and it works by interfering with cell membrane functions.[10] It is added to the water during primary disinfection (to remove pathogens) and during secondary disinfection (to avoid proliferation in the distribution system). The World Health Organization (WHO) recommends that a concentration of 0.5–5 ppm (*i.e.* mg L^{-1}) of free chlorine is maintained in the distribution system and that a minimum of 0.2 ppm is kept at the point of delivery.[11] Failure to maintain adequate free chlorine levels can have catastrophic results, as was the case during the Walkerton Tragedy (Canada), when an *E. coli* outbreak killed 7 people and infected 2300 others.[12,13]

Available technologies for online monitoring of free chlorine have been summarized in recent reviews,[8,14] but all currently accepted reference methods are based on offline procedures. There are five EPA (United States Environmental Protection Agency) approved methods for the determination of free chlorine in water.[15] They use amperometry, titrimetry, and colorimetry.[16,17] The International Organization for Standardization (ISO) has three approved methods, which rely on titrimetry and colorimetry.[18] The oxidation of *N*,*N*-diethyl-*p*-phenylenediamine (DPD) by free chlorine to generate a reddish solution and the

[a]*Department of Chemistry and Chemical Biology, McMaster University, 1280 Main Street West, Hamilton, Ontario L8S 4M1, Canada. E-mail: pkruse@mcmaster.ca*
[b]*3M Canada Company, 1840 Oxford Street, London, Ontario N5V 3R6, Canada*
[c]*Department of Mechanical Engineering, McMaster University, 1280 Main Street West, Hamilton, Ontario L8S 4L7, Canada*

† Electronic supplementary information (ESI) available. See DOI: 10.1039/d1ra08264g

subsequent measurement of the absorbance is the most popular approach to determine its concentration in water.[19–21] However, because of the extensive use of free chlorine as a disinfectant, many other quantification strategies have been reported.[14] Examples of other reagents for colorimetric detection include ABTS,[22] Michler's thioketone,[23] and syringaldazine.[24] Chemiluminescence[25–27] and fluorescence[28,29] are also successful optical sensing strategies. Multiple electrochemical sensors have also been developed, based on the principles of voltammetry[30,31] and amperometry.[4,32–34] The cited voltammetric techniques rely on the measurement of reaction products to improve sensor performance (*e.g.*, selectivity and limit of detection) thus making the process time-consuming, while the amperometric methods do so by using functionalized working electrodes. Unfortunately, the need for expensive instrumentation hinders the application of the aforementioned methods for continuous on-line monitoring. The batch-like nature of the reactions involved in the spectroscopic techniques limits them to discontinuous testing, and the consumption of reagents is a drawback. Electrochemical sensors overcome these limitations, but they are susceptible to hysteresis and fouling. Field Effect Transistors (FETs) have shown high sensitivity towards detection of free chlorine; however, the gate-voltage dependence response of the sensor as well as fabrication complexity make them not favorable for onsite or continuous measurements.[35,36]

Chemiresistive sensors are a type of electrical sensor. They work by transducing a chemical process (*i.e.* the sensing event) into an electrical signal through quantifiable changes in the conducting properties of a transducing element (*e.g.* a semiconductor).[37] Thus, the changes in resistance/conductance can be monitored by probing the devices with a constant voltage. In aqueous environments, they have successfully been used for the measurement of a range of analytes including free chlorine, pH, H_2O_2, heavy metals (Cd^{2+}, Cr^{IV}, Hg^{2+}) and organics (glycerol, TNT, atrazine).[14,38–43] Single-walled carbon nanotubes (SWCNTs) and pencil films were doped with a phenyl-capped aniline tetramer (PCAT),[44] which is readily oxidized by chlorine. The oxidation of the molecule modified the resistance of the devices, and the magnitude of the change was found to be proportional to the logarithmic scale of concentration. The sensors could be reused after being electrochemically or chemically reset. However, the need for an external reset impedes the detection of fluctuations in the concentration of free chlorine. Applications such as monitoring the integrity of filter cartridges also require a lower limit of detection, and the fabrication process is not suitable for mass production. Redox-active impurities and voids in the nanotube and pencil films may also interfere with the measurements.[45,46]

Here we report a chemiresistive sensor for the continuous monitoring of free chlorine in drinking water that uses a PCAT doped graphene-like carbon (GLC) sheet as the transducing element. We demonstrate that compared to previously published devices, GLC-based chemiresistors can be fabricated with higher consistency, operate continuously without external reset or reagents, and can be tuned in their operating range for very high sensitivity. First, we quantify the dependence of sensor performance on GLC film thickness in order to determine the optimal substrate for different applications. The sensors have a low limit of detection and do not require an external reset, allowing for the detection of fluctuations in the concentration of free chlorine over a wide dynamic range. The morphology and inert nature of the films minimize interferences from ions commonly present in drinking water. The films can be mass-produced and are easy to handle, which will facilitate a scale-up of sensor manufacturing.

Experimental section

Preparation of solutions

PCAT in its leucoemeraldine oxidation state was synthesized according to the literature.[47] Sodium thiosulphate pentahydrate (extra pure, min. 99%) was purchased from Acros Organics. Humic acid (min. 95%) and sodium phosphate dodecahydrate (ACS grade, 98.0–102.0%) were purchased from Alfa Aesar. Methanol (HPLC grade), sodium chloride (ACS grade, min. 99.0%), sodium nitrate (ACS grade, min. 99.0%), and sodium sulphate (ACS grade, min. 99.0%) were purchased from Caledon. Sodium bicarbonate (ACS grade, 99.7–100.3%) and potassium chloride (ACS grade, 99.0–100.5%) were purchased from EMD. Magnesium chloride hexahydrate (min. 99%) was purchased from Fisher BioReagents. Sodium hypochlorite solution (reagent grade, 10–15%), sodium phosphate monobasic (ACS Reagent, 98.0–102.0%), and calcium chloride dihydrate (ACS Reagent, min. 99%) were purchased from Sigma-Aldrich. All reagents were used as received. Type 1 ultrapure water (obtained with a Millipore® Simplicity® UV) was used to make all solutions. Prior to use, all glassware was pretreated for chlorine demand by soaking it in 0.1% diluted commercial bleach (Lavo-Pro 6) for an hour and rinsing it three times with ultrapure water.[48] The concentration of the free chlorine solutions was determined with the DPD colorimetric method. Both portable (Hach Pocket Colorimeter™ II) and benchtop (Thermo Scientific™ Orion™ AquaMate 8000 UV-Vis Spectrophotometer) measuring units were used. DPD Total Chlorine Reagent Powder Pillows (Hach 2105669-CA) were used with the pocket colorimeter, and the Orion™ AC4P71 Powder Chemistry Packs were used with the AquaMate.

Sensor fabrication

Polyethylene terephthalate (PET) sheets coated on one side with GLC films of different thicknesses (12, 24, 38, and 46 nm) were supplied by 3M Canada. The sheets consist of few-layer graphene platelets a few micrometres in size with some thicker nanocrystalline graphene embedded. GLC is manufactured in the absence of a binder and the platelets are deposited in a parallel fashion onto a PET substrate following a proprietary process.[49–51]

Two different device geometries were fabricated, differing only in how the transducing GLC film is brought into contact with the solutions. The basic components of the sensors are identical in both geometries (Fig. 1a). Refer to the ESI (Fig. S1†) for dimensions. The GLC-coated PET was attached to a glass

slide using double sided Kapton tape (LINQTAPE™ PIT2SD from CAPLINQ Corporation). First, one of the adhesive sides was exposed and it was carefully placed on the non-conducting side of the GLC-coated PET, avoiding the formation of wrinkles or bubbles. Using a sharp blade, the GLC-coated PET was cut around the Kapton tape. Then, the other adhesive side was exposed, and it was pasted at the end of the glass slide using gentle pressure. Next, two silver patches (PELCO® Conductive Silver Paint from Ted Pella Inc.) were painted on opposite ends of the GLC film to improve electrical contact with the copper tape. The paint was cured on a hotplate at 60 °C for 20 minutes. Finally, two pieces of copper tape (3M™ EMI Copper Foil Shielding Tape 1181 1/4 in) were pasted over the silver patches going from end to end of the glass slide.

The dip sensors (Fig. 1b) were packaged by masking the contacts with a thin layer of polydimethylsiloxane (PDMS – Sylgard® 184 Silicon Elastomer from Dow Corning). In order to prevent the PDMS from spreading over the sensing area, it was left to partially cure (approx. 6 hours at room temperature) so as to acquire a thicker consistency. Then, the contacts were masked with the thickened PDMS, and the sensors were placed on a hotplate at 60 °C until the elastomer was completely cured. For the flow sensors (Fig. 1c) a prefabricated PDMS fluidic channel was attached to the GLC. The channels were fabricated by pouring PDMS into a 3D printed mould (see ESI Fig. S1 for dimensions†). Two 1.5 cm long pieces of Masterflex® Tygon® Chemical Tubing L/S 13 (from Cole-Parmer) were cut and inserted at the inlet and outlet of the mould before pouring the PDMS. The mould was left to rest until all air bubbles disappeared and curing was then completed in an oven for 40 minutes at 80 °C. The channels were wet-bonded by spreading a thin layer of PDMS on the GLC-covered area, leaving a gap in the centre for the hollow part of the channel. The device was then placed on a hotplate at 80 °C until the PDMS was sticky. Then, the PDMS channel was carefully placed on top and the curing was finalized on the hotplate. The resistances of the sensors were in the range of 70–110 kΩ (12 nm), 2–7 kΩ (24 nm), 1.3–1.6 kΩ (38 nm), and 0.85–1.1 kΩ (46 nm). The substantial drop in resistance from 12 nm to 24 nm is due to the transition from a percolation network (Fig. 1d) to a continuous film of few-layer graphene flakes (Fig. 1e). Thicker GLC films (38 nm, 46 nm) exhibit the same continuous morphology as the 24 nm film and have a conductivity that scales directly with thickness.

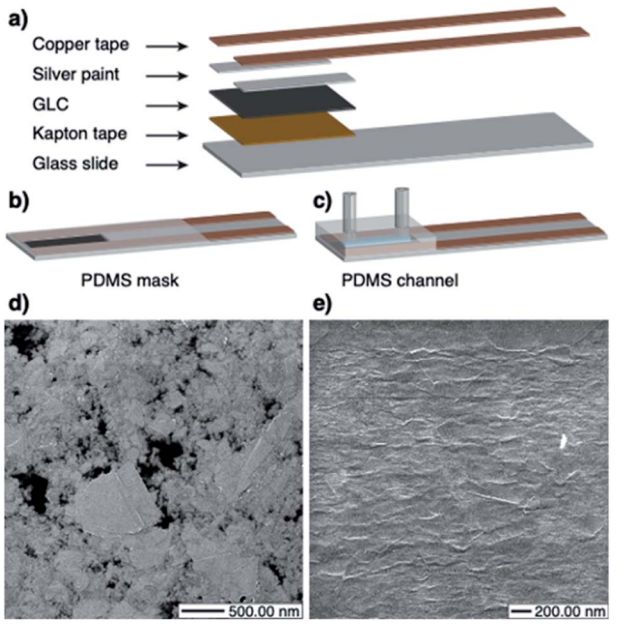

Fig. 1 (a) Basic components of the chemiresistive sensors. (b) Dip sensor geometry. (c) Flow sensor geometry. (d) Scanning Helium Ion Microscopy (HIM) image of the 12 nm GLC sheet (×32 657.14 magnification). The black areas are exposed PET substrate. (e) HIM image of the 24 nm GLC sheet (×38 000.00 magnification).

Data acquisition

In order to test the performance of the sensors, dynamic measurements of the current were taken by applying a constant potential of 10 or 100 mV across the GLC film with an eDAQ Quad Multi-Function isoPod™ (EPU452), which allows for the simultaneous monitoring of up to four sensors. The instrument was set to the Biosensor function, with a data acquisition rate of 30 min^{-1} and the maximum number of decimal places possible. To maximize resolution, the sampling range was chosen such that it was twice the amplitude of the biggest signal expected. The sample averaging period was set to 1.0 s to improve the signal-to-noise ratio. Unless noted otherwise, the noise of the signal (taken as the standard deviation of one minute of data) at the time of data collection was less than 0.5% of the total sensor response. The constant potential across the GLC film was chosen with experimental requirements in mind. While a 100 mV potential resulted in a higher current signal, a potential of 10 mV was preferred because it is important to maintain the voltage as low as possible. This way the potential drop across the portion of the chemiresistive film that is exposed to the analyte will not cause electrochemical reactions, with the two ends of the exposed films acting as two electrodes. In fact, at low biases, the electrochemical double layer acts as a rectifier and prevents current leakage through the solution. Our group has previously demonstrated free chlorine detection at 100 mV,[38] but we find 10 mV to be a conservative choice in order to avoid interferences.

For dip sensor measurements, the sensing area of the devices was immersed in a vessel containing the solution. The analyte solutions were continuously agitated using a magnetic stir bar. For flow sensor measurements, a two-channel peristaltic pump (Masterflex® L/S® Digital Miniflex Pump Systems from Cole-Parmer) was used to move the solution through the PDMS channel at a 0.2 mL min^{-1} rate. Masterflex® Tygon® Chemical Tubing L/S 13 was used for the feed. In order to study four sensors using a single pump, they were connected in series in sets of two (*i.e.*, outlet of the first sensor turns into inlet of the second sensor). Microbore PTFE tubing 1/32 inch ID (from Cole-Parmer) was used for the connections. All experiments started with a 5 minute methanol run in order to wet the channels, remove debris, reduce adventitious carbon deposits, and establish a baseline signal for doping. The set of doped sensors

followed with a 30 minute run of a methanolic solution of PCAT (5% of 7.6 mg mL^{-1}, the saturation concentration), which resulted in a significant change in signal due to the functionalization of the films. The set of blank sensors was exposed to methanol for an equivalent amount of time. The last step in the doping protocol was a 5 minute methanol rinse. Following that, all sensors were exposed to a chlorine-free aqueous background overnight in order to get a baseline before proceeding with the analyte solutions.

Scanning helium ion microscopy

The morphology of the samples was examined by Scanning Helium Ion Microscopy (HIM), which provides a higher lateral resolution (especially of surface features) and a larger depth of field than typical Scanning Electron Microscopy. An Orion Plus HIM (Carl Zeiss SMT Inc.) was employed to measure the samples. A condenser lens spot control of 4 and a beam-limiting aperture of 10 μm were chosen, giving a probe current of 0.7 pA. These experiments were conducted at WATLab (University of Waterloo).[52]

Results and discussion

Chemiresistive sensing characteristics as a function of GLC film thickness

In order to study the response of the sensors to free chlorine, increasing concentrations of the analyte solutions were run through several flow sensors. Each GLC thickness and probing voltage was studied on a separate run, with each run consisting of 2 doped sensors connected in series and 2 blank sensors connected in series. After getting a stable signal for ultrapure water, the amount of free chlorine was increased until the response of the devices was saturated (*i.e.* the response cannot be distinguished from the noise). Each solution was run for 40 minutes and the sensor response was calculated by averaging one minute of data at the 40 minute mark and comparing it to the water baseline (sensor response = $\Delta I/I_0$). The experiments were performed at biases of 10 mV and 100 mV with no effect on the results. The change in chemiresistance is not impacted by the voltage. The function of the sensor will thus not be impacted as long as the control electronics are capable of measuring sufficiently low currents (according to Ohms law), which is the case here. Fig. 2a shows representative raw data from a doped sensor (for additional data see ESI Fig. S2†).

The data was fitted to three different models: a Langmuir adsorption isotherm, an exponential decay, and a Freundlich adsorption isotherm (Fig. 2b). All of these models fit the requirement that a 0 ppm analyte concentration should lead to a 0% response. Both the Langmuir isotherm and the exponential function also incorporate asymptotic behaviour at high analyte concentrations, consistent with a saturation of the sensor response. Even though both the Langmuir and the Freundlich isotherms derive from surface science models of adsorption,[53] they cannot be applied literally to explain the sensor response, since the response may or may not be proportional to coverage. Nevertheless, they provide

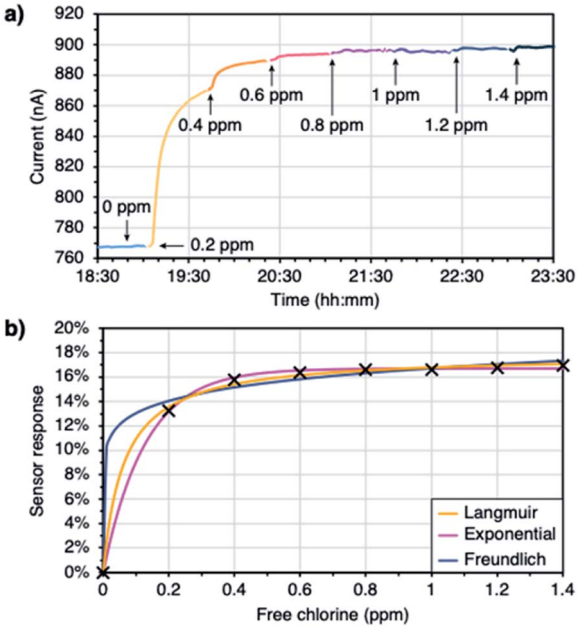

Fig. 2 (a) Raw data obtained from a doped sensor (12 nm thick GLC and 100 mV bias). (b) Calibration curves fitted to a Langmuir adsorption isotherm, exponential decay, and Freundlich adsorption isotherm.

mathematically useful models for fitting the sensor response, especially since they allow to distinguish between a scenario of coverage saturation (Langmuir) and continuing coverage increases at high concentrations (Freundlich). The equations and the curve parameters obtained with each model are gathered in the ESI (Table S1†). The Langmuir adsorption isotherm and the exponential decay provided the best fits, implying that the sensors indeed saturate in their response. From here on, Langmuir isotherms are used to discuss the performance of the devices (Fig. S3 in the ESI† gathers the curves obtained after fitting the sensor responses to the Langmuir adsorption isotherm).

As mentioned earlier, the Langmuir adsorption isotherm cannot be applied literally to explain the sensor response. In order to fit our experimental data to the model, a Langmuir-like mathematical model was used instead (eqn (1)). In that equation, y (%) is the sensor response, x (ppm) is the analyte concentration, A (%) is a curve parameter that represents the maximum sensor response, and B (ppm^{-1}) is a second curve parameter that is inversely proportional to the saturation concentration (see ESI eqn (S1) for its derivation†). These curve parameters were found to show a dependence on the thickness of the GLC. The maximum sensor response decreases as the films get thicker (Fig. 3a), while the saturation concentration increases (Fig. 3b). These trends can give insight into the sensing mechanism.

$$y = \frac{ABx}{1 + Bx} \times 100\% \quad (1)$$

Charge transfer and electrostatic gating are regarded as the dominant mechanisms underlying the sensing response of

nanocarbon sensors in aqueous solutions.[41] Other observed or proposed mechanisms include changes in gate coupling, carrier mobility changes, Schottky barriers between the nanocarbon particles (carbon nanotubes or graphene flakes) that form the percolation network that makes up the resistive film, and Schottky barrier effects at the interface between the nanocarbon film and the contacts.[54–56] We can firmly exclude the latter since the contacts are coated in the dielectric material and do not interact with the analyte (Fig. 3c). We also do not observe any correlation between the sensing signal and ionic strength (conductivity) of the analyte solution, since the electrochemical double layer at the sensor surface acts as a rectifier to block charge carrier transfer in one direction and thus prevents shunting of the chemiresistive film by the analyte solution.[57] Lastly, no substantial current will flow through the monolayer-like PCAT adsorbate layers on the doped sensors,[40] as seen in comparison to the blank devices (*i.e.* both the blank and doped devices have comparable currents). We thus conclude that the entire sensing response is due to effects within the GLC film (Fig. 3c). The data obtained as a function of GLC film thickness strongly supports the charge transfer and electrostatic gating mechanisms.

At ambient conditions, the GLC films are expected to be intrinsically p-doped.[58,59] The decrease in current observed during functionalization with PCAT can be explained through a charge transfer mechanism, as the n-doping effect of the amines lowers the number of charge carriers in the film. The free base of PCAT can be fully reduced (four amine groups), half-oxidized (two amine, two imine groups), or fully oxidized (four amine groups). As the doped sensors are exposed to free chlorine, the amines are gradually oxidized into imines and become p-type dopants, this time supplanting the intrinsic p-doping of the film.[60] Blank sensors still respond to the presence of free chlorine like they would to the presence of any oxidant in solution. The sensing mechanism of blank sensors, however, originates from the oxidation of the surface by the presence of $HOCl/OCl^-$. The oxidation induces holes to p-doped material and therefore, an increase in conductance is observed. Moreover, the presence of negatively charge free chlorine species (OCl^-) in the vicinity of the GLC can p-dope the surface through charge screening by the formed electrochemical double layer.[8,61] The resulting positive charge build-up at the sensor film surface will lead to the modulation of the sensor current as a result of an electrostatic gating effect. Oxidant solutions by definition tend to withdraw electrons from surfaces in contact with them. This is known as their redox potential, and commonly measured as a positive oxidation–reduction potential (ORP). The response of the sensors to these effects is impacted by the thickness of the films. Thinner films can only respond to smaller amounts of charge transfer and electrostatic gates (*i.e.* low concentrations) before the sensor response saturates, whereas thick films can respond to higher amounts (*i.e.* high concentrations).[62] Much thicker films, such as several hundred nanometer thick pencil drawn films, will not saturate even at very high free chlorine concentrations (above 100 ppm).[38,40] However, the impact of the charge transfer and the magnitude of the electrostatic gating effect are expected to fade into the bulk of the nanocarbon film (Fig. 3c). As a consequence, the overall response will be lower on thicker films, as a larger fraction of the current will travel through the bulk unaffected by the analyte.[63] These results suggest that the thicker the GLC film the wider the dynamic range but the lower the sensitivity (as can be seen in Fig. 3a and b). Therefore, the thickness of the film can be tailored based on the application in mind. The resistances of the films increase slightly upon immersion into water (Table 1). While water molecules themselves are not expected to cause a change in conductivity of graphene,[64] the formation of a double layer at the interface will result in electrostatic gating.[41] Higher GLC thickness results in lower resistance, confirming the bulk conductivity through the film.

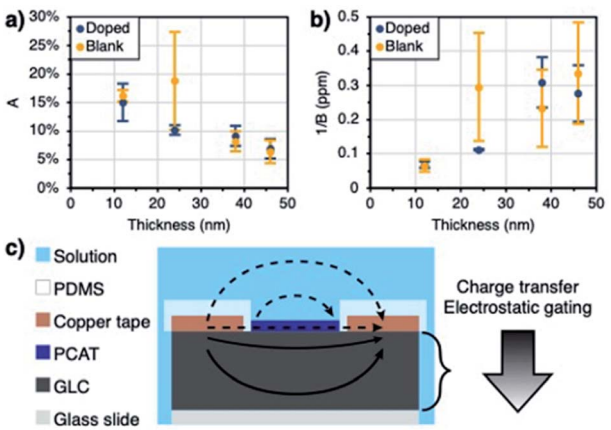

Fig. 3 (a) Thickness dependence of the maximum sensor response (10 mV). (b) Thickness dependence of the saturation concentration. (c) Proposed mechanisms for the thickness dependence of *A* and 1/*B*. The current can only travel through the bulk of the GLC film (solid arrows) as opposed to the analyte solution or PCAT molecular layers (dashed arrows). The big arrow illustrates the fading of the charge transfer and electrostatic gating effects into the bulk of the GLC.

Low range detection

The ability of the sensors to detect very low concentrations (*e.g.*, a breach in a chlorine filter) was studied next. In order to have the highest sensitivity and lowest limit of detection, 12 nm GLC was used to fabricate the devices and they were probed with

Table 1 Summary of sensor resistances in before and after exposure to water in different GLC thickness

GLC thickness	Sensor condition	Resistance – dry (kΩ)	Resistance – water (kΩ)
12 nm	Blank	31.4	32.8
	Doped	39.2	39.7
24 nm	Blank	8.76	8.72
	Doped	7.75	7.99
38 nm	Blank	1.36	1.35
	Doped	1.34	1.36
46 nm	Blank	1.11	1.12
	Doped	1.02	1.03

100 mV (2 doped sensors connected in series were run simultaneously in parallel to 2 blank sensors connected in series). The devices were exposed to increasing concentrations of free chlorine in the range of 0.01–0.2 ppm for 30 minutes each. They were reset between each concentration by running ultrapure water overnight. The response time to lower free chlorine concentrations can be reduced by adding reducing agents such as ascorbic acid or sodium thiosulphate, however, reagentless operation is preferred for water quality monitoring. Therefore, simple water resetting was preferred for this study. In cases where a faster response time is required, we have previously demonstrated resetting with a voltage applied to an auxiliary electrode.[38,39] All devices gave a pronounced signal as soon as they were exposed to free chlorine, even at the lowest concentration. The sensor response was calculated by averaging a minute of data at the 25 minute mark and comparing it to the water baseline. The response of the devices followed a Langmuir adsorption isotherm (Fig. 4a). The response of the sensors to 0.01 ppm (Fig. 4b) was pronounced enough to suggest that the detection of even lower concentrations might be possible. The limit of detection was estimated by calculating 3 times the noise and it was found to be approximately 1 ppb. More replicates can be found in the ESI (Fig. S4†), along with their respective curve parameters (Table S2†). The parameters are not comparable to those of the higher concentration range (Fig. 3a and b), indicating that the mathematical model used herein is not a perfect Langmuir adsorption isotherm. This is not surprising since there is no reason to assume that the sensor response should be strictly proportional to coverage over a wide range. A meaningful response of the devices can be obtained in less than 10 min (Fig. 4b and S4†). In the scenario of sensors being used to detect a filter breach at a point-of-use (most likely application for low concentration range), this is sufficient to alert the user to the need for changing an exhausted or gradually failing filter cartridge, while a catastrophic failure could be detected within seconds from the initial slope. The response time is thus adequate for most applications at low concentrations.

Continuous monitoring under realistic conditions

In order to study the ability of the sensors to detect fluctuations in free chlorine levels, they were exposed to multiple cycles of increasing and decreasing concentrations. Background of 100 ppm NaCl and 100 ppm $NaHCO_3$ was added to the solutions in order to simulate realistic drinking water conditions (conductivity and pH of around 320 μS cm^{-1} and 8.0 respectively, as seen in Mississauga – Ontario, Canada – drinking water).[65] Dip sensors with 24 nm GLC were used for the experiments, and they were probed with 10 mV (a single run with 3 doped sensors and 3 blank sensors connected in series). The ratio of hypochlorous acid to hypochlorite may affect the interaction of free chlorine with PCAT. Said ratio depends on the pH of the solutions, so the experimental setup included an ORP electrode (Ionode IJ-64) and a pH electrode (Fisherbrand™ accumet™ Gel-Filled Polymer Body Single-Junction pH Combination Electrode) to continuously monitor the solutions. The pH control is necessary since the chemistry of free chlorine is doubly pH dependent. At pH greater than 7.5, OCl^- is the dominant form of free chlorine while at pH lower than 7.5, HOCl is the dominant form. Furthermore, since the redox reactions of both these species involve protons (or hydroxide at high pH), there will also be a pH-dependence of their redox potential according to the Nernst equation. With increasing pH, the redox potential (*i.e.* ORP) will decrease, and the sensor response thus tends to decrease for the same concentration of free chlorine. Therefore, sensitivity will decrease and LOD will increase with increasing pH of the solution.[8,29] The concentration of free chlorine was measured by taking aliquots from the

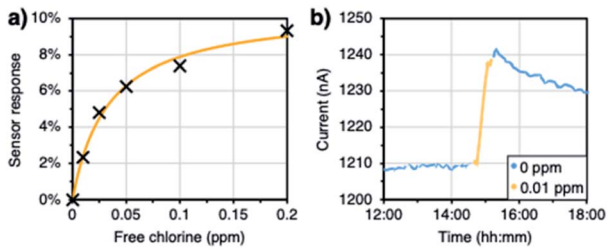

Fig. 4 (a) Response of a PCAT-doped sensor to low concentrations of free chlorine (100 mV, 12 nm GLC). (b) Raw data of one of the data points in (a) showing the response to 0.01 ppm free chlorine.

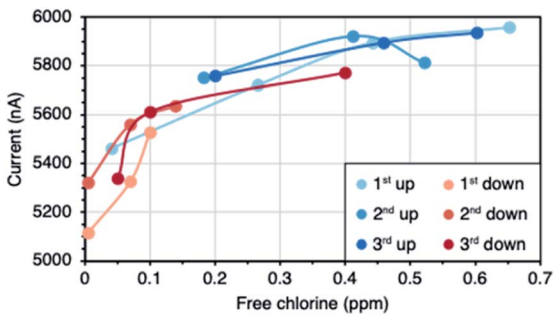

Fig. 5 Reproducibility of the detection of fluctuations in the free chlorine concentration (at 10 mV).

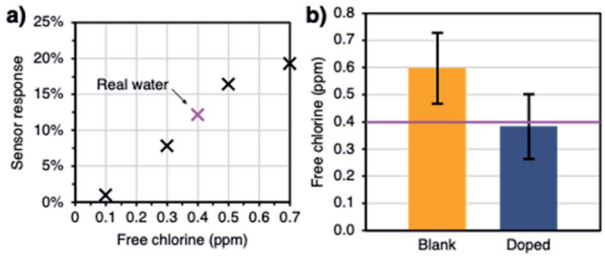

Fig. 6 (a) Doped sensor response to a real drinking water sample and subsequent spiked concentrations. (b) Averaged concentrations predicted by the blank and doped sensors. The purple line represents the real concentration of the sample, and the error bars represent the standard deviation of the sensor measurements (all measurements performed with 24 nm GLC at 10 mV).

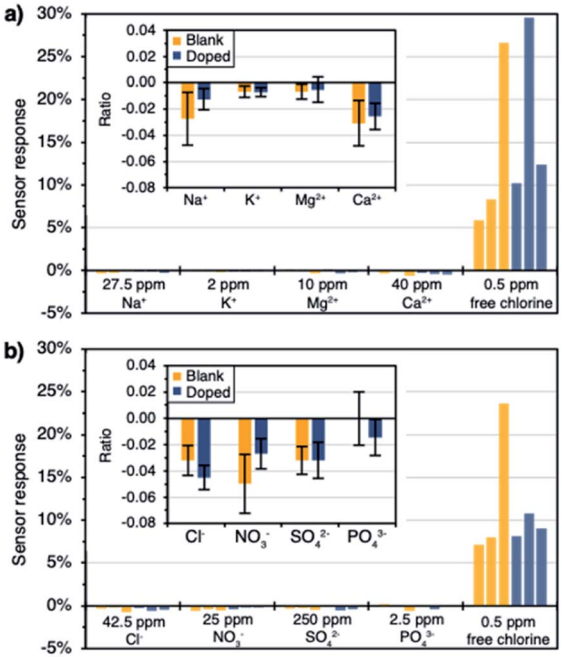

Fig. 7 (a) Cationic interference study. (b) Anionic interference study. Insets show the average responses to the interferents in proportion to the free chlorine response (all measurements performed with 24 nm GLC at 10 mV).

vessel and using the DPD method (AquaMate). For the step-ups, the solution was spiked with a stock solution of sodium hypochlorite. For the step downs, the concentration was decreased by the addition of sodium thiosulfate, which reacts with free chlorine and neutralizes it. The sensor response was calculated by averaging a minute of data after at least 30 minutes of data collection. Fig. 5 shows that the sensors respond to variations in the concentration with good reproducibility. The raw data and replicates from the other sensors can be found in the ESI (Fig. S5†). The reproducibility was found to be better in the doped devices.

The ability of the sensors to measure the concentration of free chlorine in real drinking water was also addressed. Tap water samples were collected from a residential area in Mississauga (Ontario, Canada). The drinking water supply in that location is free of chloramines, another disinfectant that could interfere with the tests. Using the same experimental setup as before, the devices were immersed in the water sample and the sensor response was calculated at the 50 minute mark. Then, the sensors were left in the solution until all the free chlorine degraded in order to obtain the baseline signal of a chlorine-free real water matrix. Finally, the sample was spiked with increasing concentrations of free chlorine (0.1–0.7 ppm) and the sensor response was calculated at the 50 minute mark. The concentrations were confirmed using the DPD method (Hach). The correlation between the response of a doped sensor and the concentration of free chlorine can be seen in Fig. 6a. Refer to the ESI (Fig. S6†) for more replicates. The data was fitted to a calibration curve and it was used to estimate the concentration of the real water sample based on the sensor response. According to Hach, the concentration of the real water sample was 0.4 ppm at the time of analysis. The doped sensors performed better at predicting the concentration (Fig. 6b).

Table 2 Comparison of recently published free chlorine sensors[a]

Sensing principle	Conductive layer	Selective species	Working range [ppm]	LOD [ppb]	Ref.
Colorimetry	—	Methyl orange	1–10	—	70
	—	DPD	0.04–6	15	71
Photo-luminescence	—	TPA	0.015–1	15	28
Chemo-luminescence	—	GQD	0.04–74	20	25
Fluorescence	—	GQD	0.02–0.5	6	72
	—	Rhodamine B@GQD	0.7–10	300	73
Amperometry	Pencil trace	Graphite	7–500	6600	74
	SnO_2 nanocolumns	GO	0.1–10	—	75
	Glassy carbon	Prussian blue	0.009–10	9	32
	Carbon	Polymelamine	0.7–520	400	76
	Glassy carbon	Polydopamine @ GO	0.7–16	3	33
	Pencil graphite	Carbamate	0.4–6	400	4
Linear sweep voltammetry	Gold *vs.* Pt; calomel ref.		0.5–4.5	10	77
	Silver *vs.* Pt; Ag/AgCl ref.		0.1–20	70	78
	Silver *vs.* Pt; Ag/AgCl ref.		1–100	2000	30
Potentiometry	Stainless steel *vs.* Pt		1–10	—	79
Solution-gated FET	Graphene	Graphene	0.07–7	7	80
Chemiresistor	CNTs	CNTs	0.03–8	—	81
	CNTs	Oligoanilines	0.06–60	—	39
	Pencil trace		0.1–60	—	40
	Pencil trace		0.06–60	—	38
	GLC	GLC or oligoanilines	0.01–1.4	1	This work

[a] LOD = limit of detection; GQD = graphene quantum dots; GO = graphene oxide; TPA = 3,5-dihydro-5-oxo-2*H*-thiazolo[3,2-*α*]pyridine-3,7-dicarboxylic acid.

Interferences

Finally, the response of the sensors towards ions commonly present in drinking water was studied (*i.e.* sodium, potassium, magnesium, calcium, chloride, nitrate, sulphate, and phosphate). The concentration of each ion was chosen based on maximum guideline values or concentrations usually found in drinking water.[66,67] Similarly to the real water experiment, a background concentration of 100 ppm NaCl and 100 ppm $NaHCO_3$ was maintained. The cationic and anionic interference studies were run separately, but they followed the same scheme. First, six dip sensors (the same set used in the previous section) were immersed in the blank solution until a stable baseline was achieved. Then, the solution was spiked with the first interferent. After an hour, the sensor response was calculated and the second interferent was added. This process was repeated until all the interferents were present (assuming no synergistic effects). Finally, the mixture was spiked with 0.5 ppm of free chlorine and the sensor response was measured at the 50 minute mark. The response of each sensor to the tested ions can be seen in Fig. 7a and b. The insets show the averaged ratios between the sensor response to the ions and the sensor response to free chlorine (taken as absolute values). All devices showed a negligible response to the tested interferents (*i.e.* response to the ion smaller than 5% of the response to free chlorine). The anions showed slightly bigger interferences than the cations, which could be due to their concentration being significantly larger. The (low) responses of both cationic and anionic interferences originate because the addition of analyte increases the ionic strength of the solution, resulting a more compact electrochemical double layer.[67] However, this sensing pathway depends on thickness and geometry of the electrical double layer and is less significant compared to the change of the redox potential at the electrode surface. Therefore, a much larger response is observed for free chlorine as compared to other interferences. We expect redox-active species such as free bromine and other disinfectants to also elicit a response of the sensors, especially for the bare sensors. We did not focus on this question here because multiple disinfectants are unlikely to coexist due to a propensity to react with each other. Usually, in practice (*e.g.*, in a drinking water distribution system), the identity of the disinfectant is known. Overall, the interferences were slightly smaller in the case of the doped sensors. Our ability to reuse the set of sensor devices from the previous set of experiments illustrates their outstanding robustness and durability.

Conclusions

We have demonstrated that GLC can be used to fabricate chemiresistive sensors for the detection of free chlorine in water over a wide dynamic range. The sensor responses were fitted to Langmuir adsorption isotherms in the two tested ranges: 0.01–0.2 ppm and 0.2–1.4 ppm. The maximum sensor response and saturation concentrations were affected by the thickness of the GLC films, with thinner films being more sensitive but having a narrower dynamic range. The limit of detection of the sensors was estimated to be as low as 1 ppb using the thinnest GLC films (12 nm). The detection of concentrations higher than 1.4 ppm might be feasible with GLC films thicker than 46 nm. The devices did not require an external reset and showed a decrease in sensor response when exposed to lower concentrations of free chlorine. Hence, they can be used to monitor concentration fluctuations. Even though the bare devices also responded to free chlorine, functionalization with PCAT improved the performance of the sensors for the quantification of free chlorine in real tap water samples. The blank devices estimated the concentration of a 0.4 ppm water sample to be 0.6 $\pm$ 0.1 ppm while the doped sensors estimated it to be 0.4 $\pm$ 0.1 ppm. The response of the sensors to cations and anions commonly found in drinking water was negligible, with the signal change being smaller than 5% of the response to 0.5 ppm of free chlorine.

Our sensors compare very favourably to the current state of the art in free chlorine sensor research (Table 2), both in terms of simplicity and limit of detection for a lower concentration range than previously reported chemiresistors. Chemiresistors are a relatively recent technology that has not yet been commercialized, so the comparison here also includes advances in other common free chlorine quantification methods based on optical, electrochemical, or electrical transduction. While offline methods are well-established, recent work has focussed on improving continuous online water quality analysis. Colorimetric,[70,71] photoluminescence,[28] chemoluminescence,[25] or fluorescence[72,73] based optical online free chlorine monitors can be optimized for high[70,73] or low[25,28,71,72] detection ranges depending on application. Detection limits around 10 ppb are comfortably achievable, but all these methods require the use of fresh reagents for each sample point. Electrochemical methods are mainly based on amperometry,[4,32,33,74–76] and linear sweep voltammetry.[30,77,78] They work reagent-less and can also achieve detection limits around 10 ppb, (3 ppb in the best case[33]) but depend on maintenance-intensive reference electrodes. Even though a potentiometric sensor has been proposed that avoids a reference electrode by using two working electrodes with dissimilar response functions, it only operates in a high detection range above 1 ppm.[79] A solution-gated FET with a 7 ppb detection limit has been demonstrated[80] but it still depends on a reference electrode. Since it was designed to be cheap and disposable, this may not be an issue for one-time measurements, but that modus operandi defeats the idea of continuous online monitoring. Chemiresistors have been demonstrated for reagentless, reference electrode free, continuous operation,[38–40,81] but struggle with resetting and work best in a high detection range ($\gg$10 ppb). This is where GLC-based chemiresistors provide a significant improvement with their reset-free operation and detection limits down to 1 ppb, in addition to the benefit that very uniform GLC films can be economically produced in large volume.

The sensitivity and dynamic range of the GLC-based chemiresistive sensors can be adjusted using different thicknesses of GLC. This opens the doors to many different applications, such as real-time water quality monitoring, the detection of breaches in chlorine filters, and the quantification of free chlorine in

unknown samples. The devices are suitable for use in remote monitoring applications due to their ultra-low power consumption of less than 100 nW (*e.g.* Fig. 5 with 24 nm film at 10 mV × 6000 nA = 60 nW) during reading (which can be intermittent). More importantly, the chemiresistive sensor design introduced here is not limited to free chlorine, as the nanocarbon films can be functionalized with probes selective to other chemicals of concern, *e.g.* cations[57,68,69] or pH.[61] In addition, we have demonstrated the use of two different sensor geometries, which expands the possibilities of sensor deployment. The manual lab-based device fabrication method employed in this study does not lend itself to achieving narrow tolerances, resulting in variations in the magnitude of response between devices. Nevertheless, we were able to demonstrate calibratable sensing behaviour on numerous devices. Inherently, the format of the GLC films will allow for low-cost mass production of sensors in the future.

Conflicts of interest

There are no conflicts to declare.

Acknowledgements

The authors would like to thank Frank Brandys of 3M Canada for useful discussions, Omar Sharif for the PCAT synthesis, Caroline Wojnas for the initial experiments, Arjun Rego for providing us with the real water samples, and Lei Zhang and Tong Leung from WATlab for the HIM data. Funding was provided by the National Science and Engineering Research Council of Canada (NSERC) through the Discovery Grant Program and a Collaborative Research and Development Grant, by 3M Canada, by the Ontario Centers of Excellence, as well as by a Canada First Research Excellence Fund project "Global Water Futures".

Notes and references

1 C. Kidgell, U. Reichard, J. Wain, B. Linz, M. Torpdahl, G. Dougan and M. Achtman, Salmonella Typhi, the Causative Agent of Typhoid Fever, Is Approximately 50,000 Years Old, *Infect., Genet. Evol.*, 2002, **2**, 39–45.

2 B. S. Fields, R. F. Benson and R. E. Besser, Legionella and Legionnaires' Disease: 25 Years of Investigation, *Clin. Microbiol. Rev.*, 2002, **15**, 506–526.

3 J. B. Kaper, J. P. Nataro and H. L. T. Mobley, Pathogenic Escherichia Coli, *Nat. Rev. Microbiol.*, 2004, **2**, 123–140.

4 S. Pan, M. L. Deen and R. Ghosh, Low-Cost Graphite-Based Free Chlorine Sensor, *Anal. Chem.*, 2015, **87**, 10734–10737.

5 F. Ramírez-Castillo, A. Loera-Muro, M. Jacques, P. Garneau, F. Avelar-González, J. Harel and A. Guerrero-Barrera, Waterborne Pathogens: Detection Methods and Challenges, *Pathogens*, 2015, **4**, 307–334.

6 M. Kaushik, A. V. Nandi and V. B. Mungurwadi, Portable Sensors for Water Pathogens Detection, *Mater. Today: Proc.*, 2018, **5**, 10821–10826.

7 M. W. LeChevallier and K.-K. Au, *Water Treatment and Pathogen Control: Process Efficiency in Achieving Safe Drinking Water*, World Health Organization, 2004.

8 Y. Qin, H.-J. Kwon, M. M. R. Howlader and M. J. Deen, Microfabricated Electrochemical pH and Free Chlorine Sensors for Water Quality Monitoring: Recent Advances and Research Challenges, *RSC Adv.*, 2015, **5**, 69086–69109.

9 C. E. Boyd, *Water Quality: An Introduction*, Springer, 2nd edn, 2015.

10 C. Venkobachar, L. Iyengar and A. V. S. Prabhakara Rao, Mechanism of Disinfection: Effect of Chlorine on Cell Membrane Functions, *Water Res.*, 1977, **11**, 727–729.

11 World Health Organization, *Guidelines for Drinking Water-Quality: Fourth Edition Incorporating First Addendum*, World Health Organization, 4th edn + 1st add, 2017.

12 M. I. Salvadori, J. M. Sontrop, A. X. Garg, L. M. Moist, R. S. Suri and W. F. Clark, Factors That Led to the Walkerton Tragedy, *Kidney Int.*, 2009, **75**, S33–S34.

13 S. E. Hrudey, P. Payment, P. M. Huck, R. W. Gillham and E. J. Hrudey, A Fatal Waterborne Disease Epidemic in Walkerton, Ontario: Comparison with Other Waterborne Outbreaks in the Developed World, *Water Sci. Technol.*, 2003, **47**, 7–14.

14 P. Kruse, Review on Water Quality Sensors, *J. Phys. D: Appl. Phys.*, 2018, **51**, 203002.

15 Office of the Federal Register, National Archives and Records Administration, *40 CFR 136 - Guidelines Establishing Test Procedures For The Analysis Of Pollutants*, Office of the Federal Register, National Archives and Records Administration, 30 Jun 2016, https://www.govinfo.gov/app/details/CFR-2016-title40-vol25/CFR-2016-title40-vol25-part136.

16 ASTM International, D1253 - 14: Standard Test Method for Chlorine in Water, in *Annual Book of ASTM Standards*, ASTM International, 2019.

17 E. W. Rice, R. B. Baird and A. D. Eaton, 4500-Cl Chlorine (Residual), in *Standard Methods for the Examination of Water and Wastewater*, ed. E. W. Rice, R. B. Baird and A. D. Eaton, American Public Health Association, American Water Works Association, Water Environment Federation, 2017, pp. 61–74.

18 International Organization for Standardization, *13.060.50 - Examination of water for chemical substances*, https://www.iso.org/ics/13.060.50/x/, accessed Jun 26, 2019.

19 A. T. Palin, The Determination of Free and Combined Chlorine in Water by the Use of Diethyl-p-Phenylene Diamine, *J. - Am. Water Works Assoc.*, 1957, **49**, 873–880.

20 L. Moberg and B. Karlberg, An Improved N,N′-Diethyl-p-Phenylenediamine (DPD) Method for the Determination of Free Chlorine Based on Multiple Wavelength Detection, *Anal. Chim. Acta*, 2000, **407**, 127–133.

21 G. Gordon, D. L. Sweetin, K. Smith and G. E. Pacey, Improvements in the N,N-Diethyl-p-Phenylenediamine Method for the Determination of Free and Combined Residual Chlorine through the Use of FIA, *Talanta*, 1991, **38**, 145–149.

22 U. Pinkernell, B. Nowack, H. Gallard and U. von Gunten, Methods for the Photometric Determination of Reactive Bromine and Chlorine Species with ABTS, *Water Res.*, 2000, **34**, 4343–4350.

23 M. Zenki, H. Komatsubara and K. Tôei, Determination of Residual Chlorine in Tap Water by Flow-Injection Spectrophotometry, *Anal. Chim. Acta*, 1988, **208**, 317–320.

24 R. Bauer and C. O. Rupe, Use of Syringaldazine in a Photometric Method for Estimating "Free" Chlorine in Water, *Anal. Chem.*, 1971, **43**, 421–425.

25 T. Hallaj, M. Amjadi, J. L. Manzoori and R. Shokri, Chemiluminescence Reaction of Glucose-Derived Graphene Quantum Dots with Hypochlorite, and Its Application to the Determination of Free Chlorine, *Microchim. Acta*, 2015, **182**, 789–796.

26 D. F. Marino and J. D. Ingle, Determination of Chlorine in Water by Luminol Chemiluminescence, *Anal. Chem.*, 1981, **53**, 455–458.

27 J. Ballesta Claver, M. C. Valencia Mirón and L. F. Capitán-Vallvey, Determination of Hypochlorite in Water Using a Chemiluminescent Test Strip, *Anal. Chim. Acta*, 2004, **522**, 267–273.

28 Q. Fang, Q. Wang, W. Lin, X. You, Y. Dong and Y. Chi, High Photoluminescent TPA and the Ratiometric Sensor for Free Chlorine, *Sens. Actuators, B*, 2017, **244**, 771–776.

29 Y. Dong, G. Li, N. Zhou, R. Wang, Y. Chi and G. Chen, Graphene Quantum Dot as a Green and Facile Sensor for Free Chlorine in Drinking Water, *Anal. Chem.*, 2012, **84**, 8378–8382.

30 M. Jović, F. Cortés-Salazar, A. Lesch, V. Amstutz, H. Bi and H. H. Girault, Electrochemical Detection of Free Chlorine at Inkjet Printed Silver Electrodes, *J. Electroanal. Chem.*, 2015, **756**, 171–178.

31 E. H. Seymour, N. S. Lawrence and R. G. Compton, Reaction with N,N-Diethyl-p-Phenylenediamine: A Procedure for the Sensitive Square-Wave Voltammetric Detection of Chlorine, *Electroanalysis*, 2003, **15**, 689–694.

32 P. Salazar, M. Martín, F. J. García-García, J. L. González-Mora and A. R. González-Elipe, A Novel and Improved Surfactant-Modified Prussian Blue Electrode for Amperometric Detection of Free Chlorine in Water, *Sens. Actuators, B*, 2015, **213**, 116–123.

33 D. R. Kumar, S. Kesavan, T. T. Nguyen, J. Hwang, C. Lamiel and J.-J. Shim, Polydopamine@electrochemically Reduced Graphene Oxide-Modified Electrode for Electrochemical Detection of Free-Chlorine, *Sens. Actuators, B*, 2017, **240**, 818–828.

34 A. van den Berg, A. Grisel, E. Verney-Norberg, B. H. van der Schoot, M. Koudelka-Hep and N. F. de Rooij, On-Wafer Fabricated Free-Chlorine Sensor with ppb Detection Limit for Drinking-Water Monitoring, *Sens. Actuators, B*, 1993, **13**, 396–399.

35 R. A. Picca, K. Manoli, E. Macchia, A. Tricase, C. Di Franco, G. Scamarcio, N. Cioffi and L. Torsi, A Study on the Stability of Water-Gated Organic Field-Effect-Transistors Based on a Commercial p-Type Polymer, *Front. Chem.*, 2019, **7**, 667.

36 C.-A. Vu and W.-Y. Chen, Field-Effect Transistor Biosensors for Biomedical Applications: Recent Advances and Future Prospects, *Sensors*, 2019, **19**, 4214.

37 A. Mohtasebi and P. Kruse, Chemical Sensors Based on Surface Charge Transfer, *Phys. Sci. Rev.*, 2018, **3**, 20170133.

38 E. Hoque, L. H. H. Hsu, A. Aryasomayajula, P. R. Selvaganapathy and P. Kruse, Pencil-Drawn Chemiresistive Sensor for Free Chlorine in Water, *IEEE Sens. Lett.*, 2017, **1**, 4500504.

39 L. H. H. Hsu, E. Hoque, P. Kruse and P. R. Selvaganapathy, A Carbon Nanotube Based Resettable Sensor for Measuring Free Chlorine in Drinking Water, *Appl. Phys. Lett.*, 2015, **106**, 063102.

40 A. Mohtasebi, A. D. Broomfield, T. Chowdhury, P. R. Selvaganapathy and P. Kruse, Reagent-Free Quantification of Aqueous Free Chlorine *via* Electrical Readout of Colorimetrically Functionalized Pencil Lines, *ACS Appl. Mater. Interfaces*, 2017, **9**, 20748–20761.

41 A. Zubiarrain-Laserna and P. Kruse, Review—Graphene-Based Water Quality Sensors, *J. Electrochem. Soc.*, 2020, **167**, 037539.

42 D. Saha, P. R. Selvaganapathy and P. Kruse, Peroxide-Induced Tuning of the Conductivity of Nanometer-Thick MoS_2 Films for Solid State Sensors, *ACS Appl. Nano Mater.*, 2020, **3**, 10864–10877.

43 P. Bazylewski, S. Van Middelkoop, R. Divigalpitiya and G. Fanchini, Solid-State Chemiresistors from Two-Dimensional MoS_2 Nanosheets Functionalized with L-Cysteine for in-Line Sensing of Part-Per-Billion Cd^{2+} Ions in Drinking Water, *ACS Omega*, 2020, **5**, 643–649.

44 E. Hoque, T. Chowdhury and P. Kruse, Chemical *in situ* Modulation of Doping Interactions Between Oligoanilines and Nanocarbon Films, *Surf. Sci.*, 2018, **676**, 61–70.

45 H. Dai, Carbon Nanotubes: Synthesis, Integration, and Properties, *Acc. Chem. Res.*, 2002, **35**, 1035–1044.

46 C. A. Gorski, M. Aeschbacher, D. Soltermann, A. Voegelin, B. Baeyens, M. Marques Fernandes, T. B. Hofstetter and M. Sander, Redox Properties of Structural Fe in Clay Minerals. 1. Electrochemical Quantification of Electron-Donating and -Accepting Capacities of Smectites, *Environ. Sci. Technol.*, 2012, **46**, 9360–9368.

47 W. Wang and A. G. MacDiarmid, New Synthesis of Phenyl/Phenyl End-Capped Tetraaniline in the Leucoemeraldine and Emeraldine Oxidation States, *Synth. Met.*, 2002, **129**, 199.

48 D. L. Harp, *Current Technology of Chlorine Analysis for Water and Wastewater*, Hach Company, 2002, p. 30.

49 R. Bauld, D.-Y. W. Choi, P. Bazylewski, R. Divigalpitiya and G. Fanchini, Thermo-Optical Characterization and Thermal Properties of Graphene–Polymer Composites: A Review, *J. Mater. Chem. C*, 2018, **6**, 2901–2914.

50 S. Ezugwu, M. S. Ahmed, R. Bauld, R. Divigalpitiya and G. Fanchini, Influence of the Addition of Graphene-like Materials on the Thermophysical Properties of Poly(3,4-Ethylenedioxythiophene):Poly(Styrenesulfonate) Thin Film Nanocomposites, *Thin Solid Films*, 2013, **534**, 520–528.

51 M. S. Ahmed, S. Ezugwu, R. Divigalpitiya and G. Fanchini, Relationship between Electrical and Thermal Conductivity in Graphene-Based Transparent and Conducting Thin Films, *Carbon N. Y.*, 2013, **61**, 595–601.
52 L. Zhang, N. F. Heinig, S. Bazargan, M. Abd-Ellah, N. Moghimi and K. T. Leung, Direct-Write Three-Dimensional Nanofabrication of Nanopyramids and Nanocones on Si by Nanotumefaction Using a Helium Ion Microscope, *Nanotechnology*, 2015, **26**, 255303.
53 I. Langmuir, The Adsorption of Gases on Plane Surfaces of Glass, Mica and Platinum, *J. Am. Chem. Soc.*, 1918, **40**, 1361–1403.
54 I. Heller, A. M. Janssens, J. Männik, E. D. Minot, S. G. Lemay and C. Dekker, Identifying the Mechanism of Biosensing with Carbon Nanotube Transistors, *Nano Lett.*, 2008, **8**, 591–595.
55 M. D. Shirsat, T. Sarkar, J. Kakoullis, N. V. Myung, B. Konnanath, A. Spanias and A. Mulchandani, Porphyrin-Functionalized Single-Walled Carbon Nanotube Chemiresistive Sensor Arrays for VOCs, *J. Phys. Chem. C*, 2012, **116**, 3845–3850.
56 K. K. Kim, S. M. Kim and Y. H. Lee, Chemically Conjugated Carbon Nanotubes and Graphene for Carrier Modulation, *Acc. Chem. Res.*, 2016, **49**, 390–399.
57 J. Dalmieda, A. Zubiarrain-Laserna, D. Ganepola, P. R. Selvaganapathy and P. Kruse, Chemiresistive Detection of Silver Ions in Aqueous Media, *Sens. Actuators, B*, 2021, **328**, 129023.
58 S. Goniszewski, M. Adabi, O. Shaforost, S. M. Hanham, L. Hao and N. Klein, Correlation of P-Doping in CVD Graphene with Substrate Surface Charges, *Sci. Rep.*, 2016, **6**, 22858.
59 K. Kanahashi, N. Tanaka, Y. Shoji, M. Maruyama, I. Jeon, K. Kawahara, M. Ishihara, M. Hasegawa, H. Ohta, H. Ago, Y. Matsuo, S. Okada, T. Fukushima and T. Takenobu, Formation of Environmentally Stable Hole-Doped Graphene Films with Instantaneous and High-Density Carrier Doping *via* a Boron-Based Oxidant, *npj 2D Mater. Appl.*, 2019, **3**, 7.
60 K. Manseki, Y. Yu and S. Yanagida, A Phenyl-Capped Aniline Tetramer for Z907/Tert-Butylpyridine-Based Dye-Sensitized Solar Cells and Molecular Modelling of the Device, *Chem. Commun.*, 2013, **49**, 1416–1418.
61 S. Angizi, E. Y. C. Yu, J. Dalmieda, D. Saha, P. R. Selvaganapathy and P. Kruse, Defect Engineering of Graphene to Modulate pH Response of Graphene Devices, *Langmuir*, 2021, **37**, 12163–12178.
62 H. Xie, K. Wang, Z. Zhang, X. Zhao, F. Liu and H. Mu, Temperature and Thickness Dependence of the Sensitivity of Nitrogen Dioxide Graphene Gas Sensors Modified by Atomic Layer Deposited Zinc Oxide Films, *RSC Adv.*, 2015, **5**, 28030–28037.
63 S. Cui, H. Pu, S. A. Wells, Z. Wen, S. Mao, J. Chang, M. C. Hersam and J. Chen, Ultrahigh Sensitivity and Layer-Dependent Sensing Performance of Phosphorene-Based Gas Sensors, *Nat. Commun.*, 2015, **6**, 8632.
64 A. D. Smith, K. Elgammal, F. Niklaus, A. Delin, A. C. Fisher, S. Vaziri, F. Forsberg, M. Rasander, H. Hugosson, L. Bergqvist, S. Schröder, S. Kataria, M. Östling and M. C. Lemme, Resistive graphene humidity sensors with rapid and direct electrical readout, *Nanoscale*, 2015, **7**, 19099.
65 Region of Peel, *Water Quality Report – Brampton, Mississauga and South Caledon (South Peel Drinking Water System)*, 2018.
66 Health Canada, *Guidelines for Canadian Drinking Water Quality – Summary Table*, Water and Air Quality Bureau, Healthy Environments and Consumer Safety Branch, Ottawa, Ontario, 2017.
67 City of Toronto, *Drinking Water Analysis Summary*, 2018.
68 J. Dalmieda, A. Zubiarrain-Laserna, D. Saha, P. R. Selvaganapathy and P. Kruse, Impact of Surface Adsorption on Metal-Ligand Binding of Phenanthrolines, *J. Phys. Chem. C*, 2021, **125**, 21112–21123.
69 J. Dalmieda and P. Kruse, Metal Cation Detection in Drinking Water, *Sensors*, 2019, **19**, 5134.
70 S. Elmas, A. Pospisilova, A. A. Sekulska, V. Vasilev, T. Nann, S. Thornton and C. Priest, Photometric sensing of active chlorine, total chlorine, and pH on a microfluidic chip for online swimming pool monitoring, *Sensors*, 2020, **20**, 3099.
71 M. Zhou, T. Li, M. Zu, S. Zhang, Y. Liu and H. Zhao, Membrane-based colorimetric flow-injection system for online free chlorine monitoring in drinking water, *Sens. Actuators, B*, 2021, **327**, 128905.
72 D. Uriarte, E. Vidal, A. Canals, C. E. Domini and M. Garrido, Simple-to-Use and Portable Device for Free Chlorine Determination Based on Microwave-Assisted Synthesized Carbon Dots and Smartphone Images, *Talanta*, 2021, **229**, 122298.
73 Y. Ding, J. Ling, J. Cai, S. Wang, X. Li, M. Yang, L. Zha and J. Yan, A Carbon Dot-Based Hybrid Fluorescent Sensor for Detecting Free Chlorine in Water Medium, *Anal. Methods*, 2016, **8**, 1157–1161.
74 J. Islam, H. Shao, M. M. R. Badal, K. M. Razeeb and M. Jamal, Pencil Graphite as Electrode Platform for Free Chlorine Sensors and Energy Storage Devices, *PLoS One*, 2021, **16**, e0248142.
75 T. Soundappan, K. Haddad, S. Kavadiya, R. Raliya and P. Biswas, Crumpled Graphene Oxide Decorated SnO_2 Nanocolumns for the Electrochemical Detection of Free Chlorine, *Appl. Nanosci.*, 2017, **7**, 645–653.
76 K. Senthilkumar and J.-M. Zen, Free Chlorine Detection Based on EC' Mechanism at an Electroactive Polymelamine-Modified Electrode, *Electrochem. Commun.*, 2014, **46**, 87–90.
77 I. Seymour, B. O'Sullivan, P. Lovera and J. F. Rohan, Electrochemical detection of free-chlorine in Water samples facilitated by *in situ* pH control using interdigitated microelectrodes, *Sens. Actuators, B*, 2020, **325**, 128774.
78 Y.-T. Chiang, S.-C. Chou, B.-Y. Sun and P.-W. Wu, A conductive silver membrane for electrochemical detection of free chlorine in aqueous solution, *Sens. Actuators, B*, 2021, **348**, 130724.

79 N. Kato, N. Hirano, S. Okazaki, S. Matsushita and T. Gomei, Development of an all-solid-state residual chlorine sensor for tap water quality monitoring, *Sens. Actuators, B*, 2017, **248**, 1037–1044.

80 C. Xiong, T. Zhang, D. Wang, Y. Lin, H. Qu, W. Chen, L. Luo, Y. Wang, L. Zheng and L. Fu, Highly Sensitive Solution-Gated Graphene Transistor Based Sensor for Continuous and Real-Time Detection of Free Chlorine, *Anal. Chim. Acta*, 2018, **1033**, 65–72.

81 L. Yang, M. Li, Y. Qu, Z. Dong and W. J. Li, Carbon nanotube-sensor-integrated microfluidic platform for real-time chemical concentration detection, *Electrophoresis*, 2009, **30**, 3198–3205.